Periodic version of the minimax distance criterion for Monte Carlo integration

ELIÁŠ, J.; VOŘECHOVSKÝ, M.; SADÍLEK, V.

Advances in Engineering Software

2020, vol. 149, November 2020, pp. 1–13

ISSN: 0965-9978

DOI: https://doi.org/10.1016/j.advengsoft.2020.102900

Accepted manuscript

Periodic version of the minimax distance criterion for Monte Carlo integration

Jan Eliáš[a,*], Miroslav Vořechovský[a], Václav Sadílek[a]

[a]*Institute of Structural Mechanics, Faculty of Civil Engineering, Brno University of Technology, Czech Republic*

Abstract

The selection of points for numerical integration of the Monte Carlo type, largely used in analysis of engineering problems, is developed. It is achieved by modification of the metric in the minimax optimality criterion. The standard minimax criterion ensures the design exhibits good space-filling property and therefore reduces the variance of the estimator of the integral. We, however, show that the points are not selected with the same probability over the space of sampling probabilities: some regions are over- or under-sampled when designs are generated repetitively. This violation of *statistical uniformity* may lead to systematically biased integral estimators.

We propose that periodic metric be considered for calculation of the minimax distance. Such periodic minimax criterion provides *statistically uniform* designs leading to unbiased integration results and also low estimator variance due to retained space-filling property. These conclusions are demonstrated by examples integrating analytical functions.

The designs are constructed by two different algorithms: (i) a new time-stepping algorithm resembling a damped system of attracted particles developed here, and (ii) the heuristic swapping of coordinates. The designs constructed by the time-stepping algorithm are attached to the paper as a supplementary material. The computer code for construction of the designs is attached too.

Keywords: numerical integration, design of experiments, space-filling designs, Latin Hypercube Sampling, Voronoï tessellation, periodic space

1. Introduction

Many engineering applications are inevitably accompanied by random nature of input variables. The randomness, arising from environment, material structure, construction process, maintenance or many other sources, needs to be properly taken into account. The resulting output of the engineering analysis is a random function and we are interested in questions which can be subsumed under the analysis of reliability, uncertainty and sensitivity. Answers to these questions are obtained by numerical integration in high dimensional parameter spaces. Such task is extremely time consuming and often becomes a bottleneck of the analysis.

We focus on this numerical integration of functions of random vectors. Let us assume a real-valued function $g(\boldsymbol{X})$ of a random vector $\boldsymbol{X} = (X_1, X_2, \ldots, X_s)$ of s elements (we assume the function is integrable and repeatable). This function can represent simple analytical formula that provides stress in elastic bent beam, a complex numerical finite element solution of a large bridge under severe condition, performance of a system or any other engineering problem. The statistical characteristics of the output are defined via s-dimensional integration

$$\mathrm{E}[S[g(\boldsymbol{X})]] = \int_{-\infty}^{\infty} \cdots \int_{-\infty}^{\infty} S[g(\boldsymbol{x})] f_{\boldsymbol{X}}(\boldsymbol{x}) \, \mathrm{d}x_1 \ldots \mathrm{d}x_s \tag{1}$$

where $f_{\boldsymbol{X}}$ is the joint probability density function of the input random vector and the statistical characteristic of interest is determined by function $S[\cdot]$. The mean value is obtained by taking $S[g(\boldsymbol{X})] = g(\boldsymbol{X})$, polynomials of $g(\boldsymbol{X})$ yield higher statistical moments provided the integrals exist. The integration is typically evaluated numerically as the weighted summation of integrand values at n discrete points. To decrease extreme computational demands, one can employ some type of surrogate model [3] or adaptive technique [23, 41]. We limit ourselves to the basic case where integration points are generated a-priori and their weights are equal to $1/n$ (the points are supposedly selected uniformly with respect to $f_{\boldsymbol{X}}$), the numerical integration can be written using the following point estimator (average)

$$\mathrm{E}[S[g(\boldsymbol{X})]] \approx \frac{1}{n} \sum_{i=1}^{n} S\left[g\left(F_{\boldsymbol{X}}^{-1}(\boldsymbol{u_i})\right)\right] \tag{2}$$

*Corresponding author
Email address: jan.elias@vut.cz (Jan Eliáš)

with $F_{\boldsymbol{X}}$ being the joint cumulative distribution function of vector $\boldsymbol{X}$, and $\boldsymbol{u}_i$ representing realizations of s independent variables with a uniform distribution spanning interval the from 0 to 1. The realizations of the original input vector $\boldsymbol{x}_i$ are obtained in Eq. (2) with the help of the inverse transformation $\boldsymbol{x}_i = F_{\boldsymbol{X}}^{-1}(\boldsymbol{u}_i)$. Therefore, the realizations $\boldsymbol{u}_i$ are drawn from a unit hypercube $\mathcal{U} = [0,1]^s$ representing the probability space. Other types of design domains are also sometimes required [11], but these are not exploited here. The selection of integration points $\boldsymbol{u}_i$ (called design points here) can be performed deterministically (via various forms of grids or quasi Monte Carlo sequences) or with some degree of randomness. In the latter case, which is explored in this paper, the result of Eq. (2) is a random variable. Its mean value should coincide with the exact solution, i.e., Eq. (2) should provide an unbiased estimator of Eq. (1). Simultaneously, the variance of the estimator should be as low as possible. These characteristics are dictated to a large extent by process in which the realizations of $\boldsymbol{u}_i$ are generated. The famous Koksma-Hlawka inequality [22, 29] postulates an upper limit for the integration error as a multiplication of the discrepancy between the set of design points $\boldsymbol{u}_i$ (called a *design* $\mathcal{D}$ hereinafter) and a term dependent solely on the integrated function.

If we have a-priori knowledge about the function, we may optimize the location of points based on that knowledge [41]. However, we focus here on a situation in which the model-free ("universal") design is created. In such a case, the Koksma-Hlawka [22, 17] inequality motivates us to use points that have low discrepancy – this property is referred to as *sample uniformity*. The research area known as *design of experiments* offers several criteria that should provide such designs based on a particular measure of discrepancy [29, 10, 40].

There is a group of point sets in the literature known as quasi Monte Carlo (QMC) sequences [14, 31, 29, 15, 45]. These sequences are designed to achieve fast decrease of discrepancy with an increasing number of points in the domain. QMC sequences are generally assumed to be the most efficient tool for numerical integration of smooth functions [44, 21, 8]. Similarly, the so-called low-dispersion sequences [30, 32] play a similar role in QMC methods for global optimization.

Another group of design criteria delivering designs with high *sample uniformity* measure space-filling property [1, 47, 46]. This group comprises several distance-based criteria among which the most famous are maximin and minimax [19], Audze-Eglājs [1] and ϕ_p (known as phi criterion) [28]. For an overview of the design of experiments please see, e.g., the recent review paper [12].

Designs optimized with respect to discrepancy or space-filling criteria indeed exhibit reduced estimator variability. However, this is not a sufficient condition for unbiased Monte Carlo integration. Eq. (2) is derived from the assumption that every possible domain point has the same probability of being included in the design. This *statistical uniformity* is usually violated in standard space-filling criteria, as has been shown by authors for Audze-Eglājs in [9] and for maximin and ϕ_p criteria in [49]. Vořechovský and Eliáš [49] also show the statistical non-uniformity of the widely used centered L_2 discrepancy [16] and recently proposed *support points* [24].

A simple remedy which is and easy to implement was also proposed in [9, 49] for distance-based criteria to ensure their *statistical uniformity* via the usage of periodic space. The same idea is expanded here for the minimax criterion and conceptually for its relaxed version.

Besides designs from $\mathcal{U}$, we will also consider Latin hypercube (LH) designs [6, 27] in the unit hypercube, i.e., the location of points will be limited to the finite set $\mathcal{L} \in \mathcal{U}$, $\mathcal{L} = \left\{ \left(i - 1/2\right)/n \right\}^s$ for $i \in \{1, 2, \ldots, n\}$, and each coordinate value must be used exactly once for each dimension. The fundamental concepts of this paper can be applied to LH designs from the finite set $\mathcal{L}$ as well as to designs from the infinite set $\mathcal{U}$, but LH designs are particularly attractive because they are non-collapsing and also represent each input variable in an optimal manner.

2. The standard minimax criterion ϕ_{mM}

Let us consider a design $\mathcal{D}$ with n points $\boldsymbol{u}_i$. The minimax optimal design, $\mathcal{D}_{\mathrm{mM}}$, minimizes the maximum distance from an arbitrary point $\boldsymbol{u} \in \mathcal{U}$ to the nearest design point $\boldsymbol{u}_i$ [19]. To find such a design, one needs to search for $\mathcal{D} = (\boldsymbol{u}_1, \boldsymbol{u}_2, \ldots, \boldsymbol{u}_n)$ so that the minimax measure ϕ_{mM} is minimized

$$\phi_{\mathrm{mM}}(\mathcal{D}) = \max_{\boldsymbol{u}\in\mathcal{U}} \left[\min_{i=1\ldots n} d\left(\boldsymbol{u}, \boldsymbol{u}_i\right) \right] \tag{3}$$

A more appropriate name for the criterion would therefore be the minimaximin criterion, as noted by Pronzato and Müller [35]. The function d can be an arbitrary metric; typically Minkowski distance is used

$$d_r(\boldsymbol{u}_i, \boldsymbol{u}_j) = \left(\sum_{v=1}^{s} \left[\Delta_v(\boldsymbol{u}_i, \boldsymbol{u}_j)\right]^r \right)^{1/r} \tag{4a}$$

$$\text{where} \quad \Delta_v(\boldsymbol{u}_i, \boldsymbol{u}_j) = |u_v^i - u_v^j| \quad \text{and} \quad r \geq 1 \tag{4b}$$

with $r = 1$ (Manhattan distance), $r = 2$ (Euclidean distance) or $r = \infty$ (Chebyshev distance) [47]. Only Euclidean distance is considered further in this paper, as the application of other powers in Minkowski distance

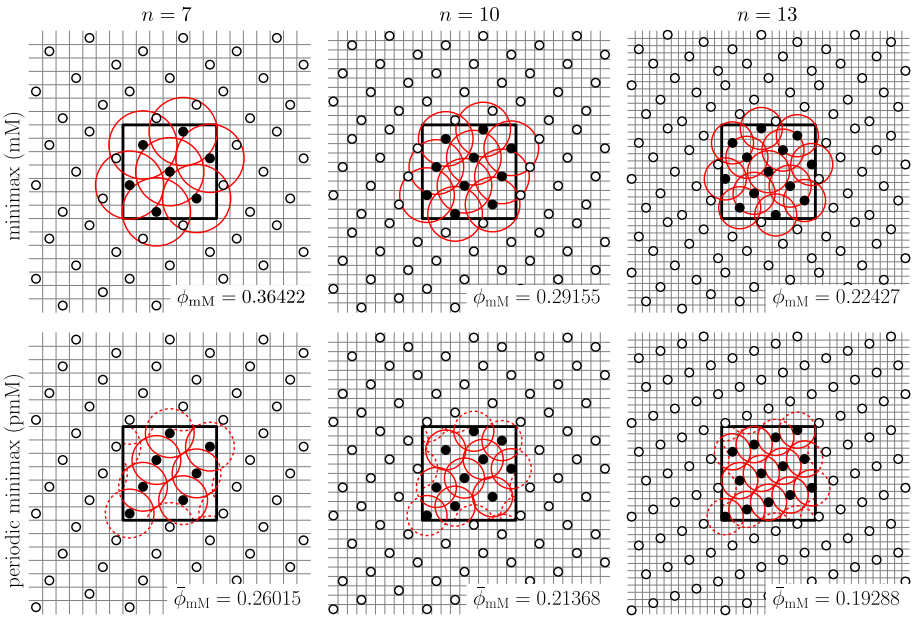

Figure 1: Optimal designs with respect to the minimax criterion (top row, designs taken from https://spacefillingdesigns.nl) and the proposed periodic minimax criterion (bottom row) for $s = 2$ and n =7, 10 and 13. The red circles with centers at the design points have a radius equal to the $\phi_{\mathrm{mM}}(\mathcal{D})$ or $\bar{\phi}_{\mathrm{mM}}(\mathcal{D})$ value of that particular design and demonstrate the design's quality – the whole domain must be covered by the circles but overlapping should be minimized.

is straightforward. Euclidean distance is isotropic, i.e., the distance between two points does not depend on the orientation of the coordinate axes. However, its usage in a higher dimensional hypercube is problematic due to the concentration of distances [39].

The search for $\mathcal{D}_{\mathrm{mM}}$ is also known as the facility location problem or the set covering location problem [43]. It has a number of practical applications such as the creation of an ozone monitoring network [37]. The seminal paper by Johnson et al. [19] showed that the minimax design is G-optimal for certain correlation structures, i.e., it minimizes the maximum Kriging variance. It is therefore often used to find designs optimal for the construction of emulators.

Eq. (3) can be relaxed analogously to the way the maximin criterion was relaxed to formulate the ϕ_p criterion. The relaxation replaces strict requirement of Eq. (3) to minimize only the maximum distance to minimization of an integral of distances raised to some power over the whole domain. A family of new criteria is produced by the relaxation [37]

$$\phi_{\mathrm{mM}[p,q]}(\mathcal{D}) = \left(\int_{\mathcal{U}} \left[\sum_{i=1}^{n} d(\boldsymbol{u}, \boldsymbol{u}_i)^{-q} \right]^{-p/q} \mathrm{d}\mathcal{U} \right)^{1/p} \tag{5}$$

with $p, q > 0$. The minimax criterion is recovered for $p, q \to \infty$.

Examples of minimax optimal LH designs in two dimensions with Euclidean distance for $n = 7$, 10 and 13 are shown in the top row of Fig. 1. These designs were taken from the database https://spacefillingdesigns.nl [47]. The *sample uniformity* (or space-filling property) guaranteed by the design criterion is achieved. However, it will be shown below that the *sample uniformity* is not maintained and therefore these designs result in biased integration.

3. The periodic minimax criterion $\bar{\phi}_{\mathrm{mM}}$

Inspired by our work on the Audze-Eglājs, maximin and ϕ_p criteria [9, 49], we propose a *periodic* version of the minimax criterion. We start with a periodic Euclidean metric $\bar{d}$

$$\bar{d}(\boldsymbol{u}_i, \boldsymbol{u}_j) = \sqrt{\sum_{v=1}^{s} \left[\bar{\Delta}_v(\boldsymbol{u}_i, \boldsymbol{u}_j)\right]^2} \tag{6a}$$

where

$$\bar{\Delta}_v(\boldsymbol{u}_i, \boldsymbol{u}_j) = \min\left\{\Delta_v(\boldsymbol{u}_i, \boldsymbol{u}_j), 1 - \Delta_v(\boldsymbol{u}_i, \boldsymbol{u}_j)\right\} \tag{6b}$$

The periodic metric measures distance in the periodic space defined by the unit hypercube $\mathcal{U}$. It considers all the periodic images of points at coordinates $\boldsymbol{u} + \boldsymbol{k}$, with $\boldsymbol{k}$ being a vector of arbitrary integers ($\mathbb{Z}$) of size s,

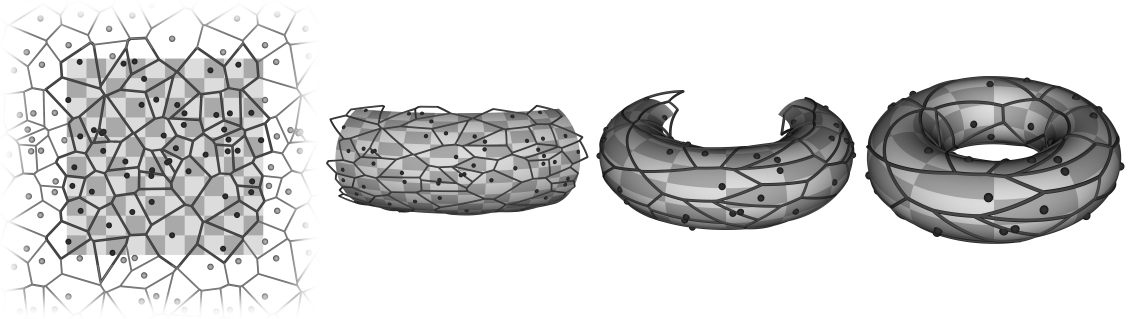

Figure 2: Visualization of periodic Voronoï tessellation on a unit square and its folding into a torus, n =50.

but only the shortest distance among all the images is taken into account. This type of periodic space is often referred to as the *minimum image convention*. Plugging the periodic metric into the definition of the minimax distance criterion from Eq. (3) provides its periodic version

$$\overline{\phi}_{\mathrm{mM}}(\mathcal{D}) = \max_{\boldsymbol{u}\in\mathcal{U}} \left[\min_{i=1\ldots n} \overline{d}\left(\boldsymbol{u}, \boldsymbol{u}_i\right) \right] \tag{7}$$

which is called the periodic minimax criterion hereinafter. Examples of periodic minimax optimal LH designs are shown in the bottom row of Fig. 1, including the nearest periodic images of all the design points. One can see that the space-filling property (*sample uniformity*) of the design is preserved.

To prove that the *statistical uniformity* is ensured, imagine an arbitrary shift of the whole design $\mathcal{D}$ by a vector $\boldsymbol{l}$ of arbitrary real numbers (without a loss of generality limited to interval $\langle 0, 1\rangle$) of size s. Whenever a point leaves the hypercube, it enters it again from the opposite side due to the periodicity. Thus the individual coordinates of the new points will be either $u_v + l_v$ or $u_v + l_v - 1$. For all possible variants, the quantity $\overline{\Delta}$ from Eq. (6b) is always preserved for every dimension, implying that the periodic distance between any two points is preserved as well. Therefore, $\overline{\phi}_{\mathrm{mM}}(\mathcal{D})$ is invariant with respect to an arbitrary shift. When a design is $\overline{\phi}_{\mathrm{mM}}$ optimal, so are all its shifted versions, and all of them have the same probability of being found in the optimization process (assuming the optimization process itself is unbiased). Therefore, all the locations share the same probability of being selected and the design is *statistically uniform*.

If the metric imposed by Eq. (6) were used in the relaxed version of the minimax criterion from Eq. (5) then the periodic relaxed version would be obtained. It would only be approximative, since only the shortest distances are considered – not all periodic images. The error would be greater for low powers q, for which the ignored distances to other periodic images of $\boldsymbol{u}_i$ contribute significantly. In any case, the periodic minimax distance from Eq. (7) is exact, since only the shortest distances contribute.

4. Evaluation of ϕ_{mM} and $\overline{\phi}_{\mathrm{mM}}$

The evaluation of the minimax criterion (Eq. 3) is relatively computationally expensive. If one has a design $\mathcal{D}$ with design points $\boldsymbol{u}_i$, one needs to solve the maximization problem by finding the location $\boldsymbol{u}^* \in \mathcal{U}$ with the largest distance from the design points. In the literature one can find three approaches which can be used to determine the location of $\boldsymbol{u}^*$:

- Typically, the problem is approximated by limiting the candidates for $\boldsymbol{u}^*$ to a finite set of points chosen artificially (usually a regular grid). This is the most common method that allows $\phi_{\mathrm{mM}}(\mathcal{D})$ to be estimated in reasonable time. However, to keep the error of such an estimate low, the grid needs to be dense and the number of candidate points in the grid grows fast with dimension s. The modification of this method for periodic space is easy: one can use the same grid and the same evaluation method; it suffices to replace the metric d with the periodic version $\overline{d}$.

- Another option for the evaluation of $\phi_{\mathrm{mM}}(\mathcal{D})$ is via what is known as Markov chain Monte Carlo optimization. It is a sequential construction of points placed randomly but at a decreasing distance from design points $\boldsymbol{u}_i$. As the distance decreases, the ϕ_{mM} value is estimated with diminishing error. The algorithm is thoroughly described in [13]. Pronzato [34] shows that this method is the most effective for higher dimensions (tested up to $s = 5$) as the computational time increases linearly with s. The periodic version is again straightforward; as before, it suffices to change the metric to $\overline{d}$.

- The last method uses Delaunay triangulation and/or Voronoï tessellation. These dual methods essentially directly identify candidates for $\boldsymbol{u}^*$. In the case of Delaunay triangulation, the $\phi_{\mathrm{mM}}(\mathcal{D})$ is the radius of the largest hypersphere that is circumscribed to Delaunay simplices, while in the case of Voronoï tessellation, the $\phi_{\mathrm{mM}}(\mathcal{D})$ is the maximum distance of the Voronoï vertex to the design points $\boldsymbol{u}_i$. This method yields

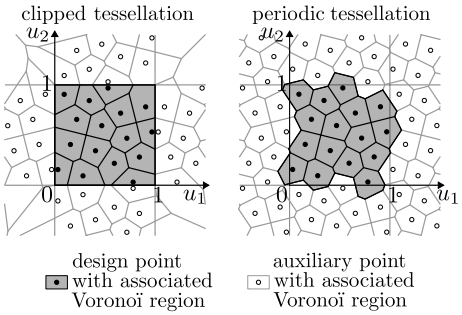

Figure 3: Clipped and periodic Voronoï tessellations for $s = 2$ and n =16.

exact results as the set of candidates for $\boldsymbol{u}^*$ determined by the tessellation or triangulation contains the true solution. Unfortunately, the computational complexity of Delaunay triangulation and Voronoï tessellation becomes prohibitive for higher dimensions. In addition, the Voronoï tessellation can be constructed only approximately, as is effectively done in [26]. However, the method then becomes essentially the same as the first method on this list.

One also needs to properly analyze the boundary region of the tessellation/triangulation. Both the Delaunay triangulation and Voronoï tessellation approaches do not provide candidates for $\boldsymbol{u}^*$ at the boundary of the hypercube, so they must be found by additional geometrical calculations [7]. As the boundary region occupies more volume for high s, such additional calculations may take a significant time. One can easily get rid of the problems with boundaries by extending n points by their *symmetric* images with respect to all hypercube boundaries [35], i.e., by calculating triangulation on $n(2s + 1)$ points. Even if not all n symmetric images are considered, the computational complexity still grows fast with s.

The modification for the periodic minimax distance is in this case more elaborative since the boundaries must be treated in a completely different, periodic way. One can imagine it as computing Voronoï tessellation or Delaunay triangulation in a folded space (anuloid), see Fig. 2 or Fig. 3. The next section elucidates the developed algorithm for such a construction.

Since the third method is the only exact one, we decided to employ it for the evaluation of both the minimax (ϕ_{mM}) and the periodic minimax ($\overline{\phi}_{\mathrm{mM}}$) criteria. The Voronoï tessellation with auxiliary points placed symmetrically (mirrored) with respect to all the boundaries (needed for the calculation of ϕ_{mM}) is often called *clipped* in the computational geometry literature [54]. There are also papers computing the *periodic* Voronoï tessellation needed for the calculation of $\overline{\phi}_{\mathrm{mM}}$. However, these algorithms are usually focused on centroidal Voronoï tessellation in $s = 2$ or $s = 3$ dimensions and complex, often nonconvex regions as the application is the generation of meshes [53, 38, 42]. In our case, we would like to compute clipped and periodic tessellation in higher dimensions, but our region is a simple convex hypercube. For that reason, we have developed our own algorithm employing Q-hull code [2].

4.1. Incrementally constructed clipped Voronoï diagram

The *clipped* version starts by placing *auxiliary* outside points symmetrically with respect to all the boundaries. One can mirror all the n inner points to make sure the correct solution will be obtained. However the calculation of the tessellation is then performed with $n+2sn$ points, which can be unnecessarily time consuming. We therefore mirror only the N_0 points that are closest to each mirroring plane. The solution is then computed on $n + 2sN_0$ points only, which can be much faster, though it may happen that the result is not fully correct. The incorrect solution is enriched by the subsequent mirroring of additional points in a loop until the correct solution is found.

The correctness of the solution and additional auxiliary points are determined via Delaunay simplices. All the simplices that connect inner (original) and outer (auxiliary) points are selected. It is required that each inner point of such a simplex is symmetrically placed with respect to all the boundaries crossed by that simplex. If such a point is missing, it is added in the next step. If no auxiliary point is missing, we have the correct *clipped* Voronoï tessellation. An example of this procedure is shown in Fig. 4 left with $n = 16$ points and $s = 2$ dimensions. The gray color marks all the simplices that cross boundaries but do not have all of their inner points mirrored. Four new auxiliary points are identified and the triangulation/tessellation is updated. The tessellation in the second step is already the correct solution.

Based on trial–error analyses, the reasonable N_0 was estimated as $N_0 = 3n\ell_{\mathrm{char}}$, where the characteristic length $\ell_{\mathrm{char}} = n^{-1/s}$ represents the shortest distance in the regular orthogonal grid [39]. The procedure usually terminates in the second step, but sometimes more steps are needed. Though Q-hull software allows the incremental extension of sets of points and the updating of the solution, it has been found to be much quicker to delete the previous solution and compute the new one from scratch.

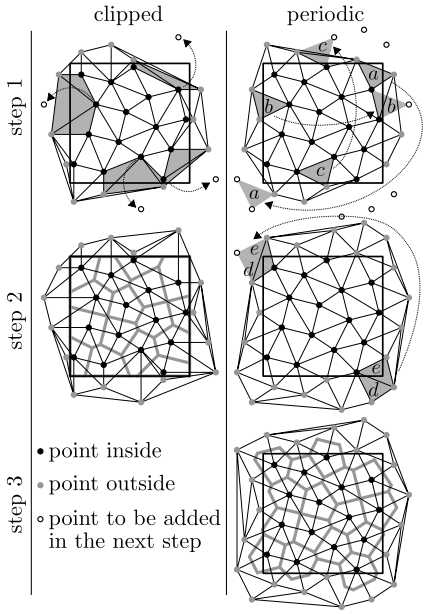

Figure 4: Incremental construction of *clipped* and *periodic* Voronoï tessellations and Delaunay triangulation for $s = 2$ and n =16.

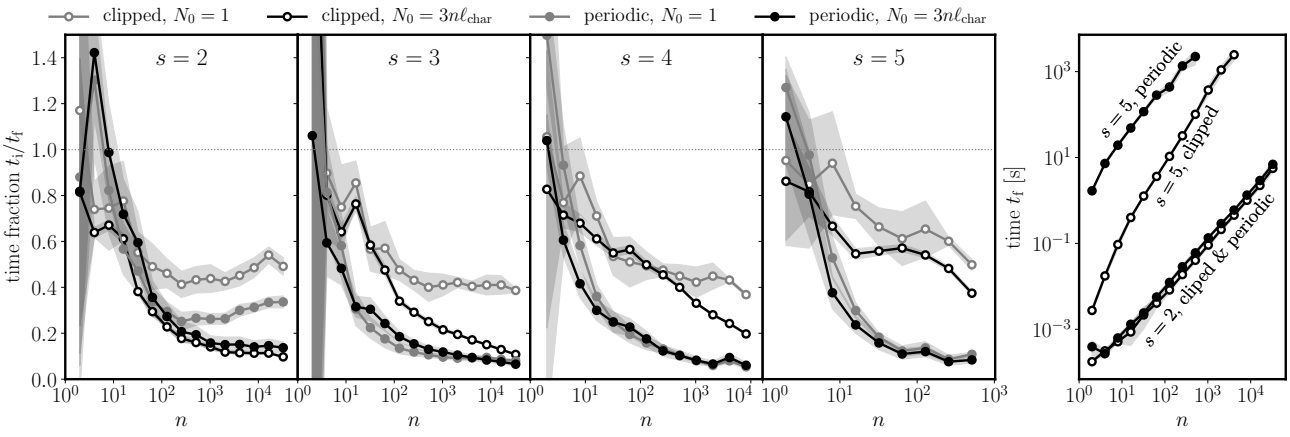

Figure 5: Performance of the incremental construction of *clipped* and *periodic* Voronoï tessellations using $N_0 = 1$ and $3n\ell_{\text{char}}$ initially reflected or periodically repeated points. The four graphs on the left report the computational time of the incremental solution, t_i, divided by the computational time of the full solution, t_f, measured when all the inner points are reflected or periodically repeated in all necessary directions. The right-hand graph shows real time t_f for $s = 2$ and 5. The Voronoï constructions for each case were repeated 50 times with different locations of design points. Solid lines with circular markers show averages based on those 50 repetitions, while shaded bands show averages ± standard deviations.

4.2. Incrementally constructed periodic Voronoï diagram

For *periodic* tessellation, the mirroring is replaced by periodic repetition of the N_0 points that are closest to the boundaries. Unfortunately, one also needs to add auxiliary periodic images of points in the "corner regions", i.e., in all regions where two or more coordinates are above 1 or below 0. This is ignored in the first step, however, and the first Voronoï tessellation is found for n (inner) plus $2sN_0$ (outer) points.

The solution must again be checked for correctness. Whenever any simplex crosses a boundary hyperplane, it is required that all its inner points be periodically repeated with respect to the crossed boundaries. Otherwise, the missing points are added in the next step. The situation is shown in Fig. 4 right, where some (not all) of these simplices are colored in gray. Simplices b and c simply cross one boundary, and thus must be periodically repeated with respect to this boundary. Simplices a, d and e require periodic repetition with respect to two boundaries. In the third step we find the correct solution.

Once again, the algorithm seems to work well for $N_0 = 3n\ell_{\text{char}}$, and the fastest Q-hull implementation compute a completely new solution in every step. Usually more than two steps are needed.

A comparison of approximate computation times for the incremental algorithm (t_i) and full solution (t_f) in several dimensions is shown in Fig. 5. The full solution assumes the mirroring or periodic repetition of all the points directly (a total of $n(2s + 1)$ points for the *clipped* and $n3^s$ points for the *periodic* tessellation). The results show that the full solution is only faster for extremely low n.

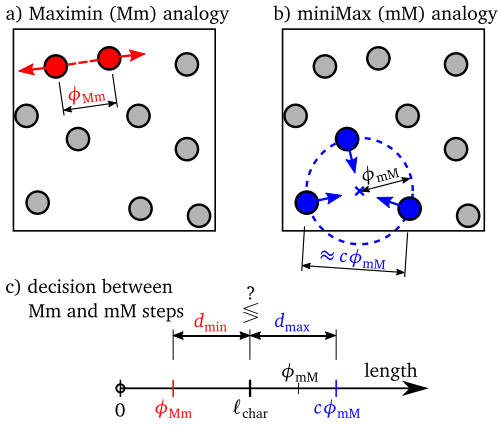

Figure 6: Illustration of the analogies between distance-based criteria and a system of particles. a) Mm step. b) mM step. c) Decision between the two types of steps in the initial rearrangement.

5. Construction of minimax optimal designs

The search for an optimal minimax design is an extremely difficult problem. Even if we restrict ourselves to the LH sampling, the finite set of options has size $(n!)^{s-1}/(s-1)!$ (if we ignore permutation of coordinates). The exhaustive search method quickly becomes prohibitively time-consuming, even for $s = 2$. Instead, heuristic optimization methods that, unfortunately, often deliver only the local minimum are being used. Some possible optimization methods are listed in [34]. In this paper, one existing and one new method are employed.

5.1. Shuffling of coordinates based on simulated annealing

In our previous papers [9, 49] focused on different design criteria we used a heuristic optimization method based on simulated annealing [20, 5]. A thorough description of the algorithm can be found in [50]. Starting with a random LH design, new trial designs are generated by swapping a randomly chosen coordinate v of a randomly chosen pair of points a and b: $u_v^a \rightleftarrows u_v^b$. The swap is accepted based on the difference in the minimax distance value of the original and new designs $\Delta\phi_{\mathrm{mM}} = \phi_{\mathrm{mM}}(\mathcal{D}_{i+1}) - \phi_{\mathrm{mM}}(\mathcal{D}_i)$ with a probability based on the Boltzmann distribution

$$P = \begin{cases} 1 & \Delta\phi_{\mathrm{mM}} \leq 0 \\ \dfrac{1}{1+\exp\left(\Delta\phi_{\mathrm{mM}}/t\right)} & \Delta\phi_{\mathrm{mM}} > 0 \end{cases} \tag{8}$$

For the periodic version, the criterion $\overline{\phi}_{\mathrm{mM}}$ is used. Temperature t governs the process and decreases throughout it from the initial to the final temperature in steps. At each temperature step, a user defined number of trial swaps is performed.

Simulated annealing is a heuristic optimization technique in which ϕ_{mM} or $\overline{\phi}_{\mathrm{mM}}$ are typically calculated hundreds of thousands of times. In the case of the minimax or periodic minimax criteria, the computational burden associated with so many evaluations is huge, and the temperature evolution and number of trial swaps at each temperature step (known as the *cooling schedule*) needs to be drastically modified to reduce the number of evaluations of the criteria. The price paid for such a reduction is that only near-optimal solutions are found.

5.2. Time-stepping algorithm for the construction of distance-based designs

The insufficient performance of the switching algorithm for the minimax criterion resulted in the development of a completely new optimization method. Vořechovský et al. [51] argued that the distance-based criteria for a design consisting of n points can be viewed in analogy with a system of n particles in s-dimensional space: the particles, each having s coordinates, represent the design points. Various formulas for the optimality criteria involve terms for all pairs of points, and these terms can represent the pairwise potential energy. Given this analogy, designs can be constructed by minimizing the total potential energy of a system of particles via the dynamical simulation of an N-body system [25]. As argued in [51], the (periodic) minimax criterion provides potential that changes abruptly and is therefore not suitable for a fully dynamic solution. Instead, this paper proposes a simplified version of the dynamical algorithm that neglects particle inertia and is well suited for the maximin and minimax criteria. It can employ the *intersite* and *periodic* metric equally well.

At the beginning, a random arrangement of particles is generated. The simulation proceeds in time *steps* in which only selected particles i are displaced from their current positions: $\boldsymbol{u}_i(t+\Delta t) = \boldsymbol{u}_i(t) + \boldsymbol{s}_i(t)$. The magnitude of the displacement (the Euclidean length of the steps $\boldsymbol{s}(t)$) decreases with increasing step number (time t). When the miniMax (mM) criterion is to be minimized, up to $(s+1)$ particles lying on the surface of the largest empty hypersphere (forming the critical simplex) are displaced towards the center of this hypersphere. In

such a new configuration, the criterion is recalculated by identifying the current critical simplex and displacing its points. The displacements depend only on the current positions; no information from the previous step is utilized (one can think of neglected inertia in a dynamical system of particles). Such a displacement is called the mM-step and is illustrated in Fig. 6b. Similarly, when the maximin (Mm) criterion is targeted, the individual steps proceed by selecting the nearest pair of particles and moving the two particles in opposite directions (see Fig. 6a for an illustration).

Experience shows that when an algorithm solely employs a series of mM-steps, particle clusters typically appear as there are no repelling forces between the particles. Analogously, when the algorithm involves a sequence of Mm-steps only, clusters are eliminated but large empty regions may remain unfilled. Therefore, before imposing the target criterion, we recommend always performing *initial rearrangement* by alternating both types of steps. The type of step to be performed is selected based on the comparison of two current length parameters: $d_{\min}$ and $d_{\max}$. The definitions of these lengths are: $d_{\min} = |\ell_{\text{char}} - \phi_{\text{Mm}}|$ and $d_{\max} = |c\,\phi_{\text{mM}} - \ell_{\text{char}}|$, where ϕ_{Mm} is the Maximin criterion, i.e., the smallest pairwise distance, ϕ_{mM} is the radius of the largest empty hypersphere and $c = \sqrt{2(s+1)/s}$ is the ratio between the circumradius and the edge length of a regular simplex (for the periodic version replace ϕ_{mM} and ϕ_{Mm} with $\bar{\phi}_{\text{mM}}$ and $\bar{\phi}_{\text{Mm}}$). When $d_{\min} > d_{\max}$, the spreading of the cluster is applied (Mm-step), otherwise the shrinking mM-step is taken.

Once the initial rearrangement is finished, the algorithm can proceed with a series of steps of a single type depending on the target criterion. In order to increase the robustness of the algorithm, we recommend always applying a small random perturbation to each point in a random direction after performing a certain number of steps. The magnitudes of these perturbations also decrease with the number of steps (analogously to the decreasing excitations in annealing due to decreasing temperature). Even though these perturbations usually increase the value of the criterion, they can help to prevent locking in a local minimum. Once the final configuration is reached, the coordinates of the points are taken as the design.

It is worth noting that the periodic version of the time-stepping algorithm typically finds the solution faster than the intersite version. The intersite version is constrained by boundaries and more point displacements are needed to satisfy these constraints. In contrast, the periodic version is unconstrained and progressively develops towards the "closest" of all the shifts of the optimal pattern with the lowest minimax criterion.

If LH design is desired, a postprocessing step must be taken in order to distribute the coordinates uniformly along each dimension. The predefined coordinates are selected as midpoints of n segments of the unit length: $(\pi_i - 1/2)/n$, where the integers π_i are the rank numbers of points along the current coordinate. We remark that the latinized sample obtained with "free points" may not necessarily be the best possible LH sample given the ϕ_p criterion. However, the application of latinization via post-processing in this manner is much more efficient than the combinatorial optimization that shuffles predefined coordinates based on the simulated annealing algorithm described in Sec. 5.1.

5.3. Comparison of SA and TS algorithm performance

The designs generated by the simulated annealing (SA) and time-stepping (TS) algorithms are compared from the viewpoint of the following criteria: the (i) standard minimax, (ii) periodic minimax, (iii) periodic phi criterion with power $p = s + 1$ and (iv) wrap around discrepancy. We intend to show via such comparison the versatility of the proposed periodic minimax criterion: it provides designs with relatively good quality also with respect to criteria for which they were not directly optimized.

We also intend to compare performance of the $\bar{\phi}_{\text{mM}}$ designs with random designs or designs optimized by other criteria from the literature. The designs under comparison are:

- random LH designs as a reference solution.
- a quasi Monte Carlo (QMC) sequence used widely for numerical integration. From the pool of available QMCs we have selected the Sobol' sequence. The sequence is generated from the R package "`fOptions`" [36, 52] using the "`runif.sobol`" function.
- optimal minimax and periodic minimax designs obtained by simulated annealing (denoted ϕ_{mM} LH SA and $\bar{\phi}_{\text{mM}}$ LH SA, respectively). These designs are optimized in 2 and 3 dimensions only due to their heavy computational demands, and they are limited to the $\mathcal{L}$ space.
- optimal minimax and periodic minimax designs obtained by a time-stepping algorithm without latinization (denoted ϕ_{mM} TS and $\bar{\phi}_{\text{mM}}$ TS, respectively). The effectiveness of the time-stepping algorithm allows optimization even in dimension 5, but we only studied it up to $n = 512$ points.
- latinized designs from the previous item (denoted ϕ_{mM} LH TS and $\bar{\phi}_{\text{mM}}$ LH TS, respectively).
- optimal periodic phi LH designs (labeled $\bar{\phi}_{s+1}$ LH) obtained by simulated annealing optimization with the distance exponent $p = s + 1$. These designs were presented in [49] and are included here for comparative purposes.

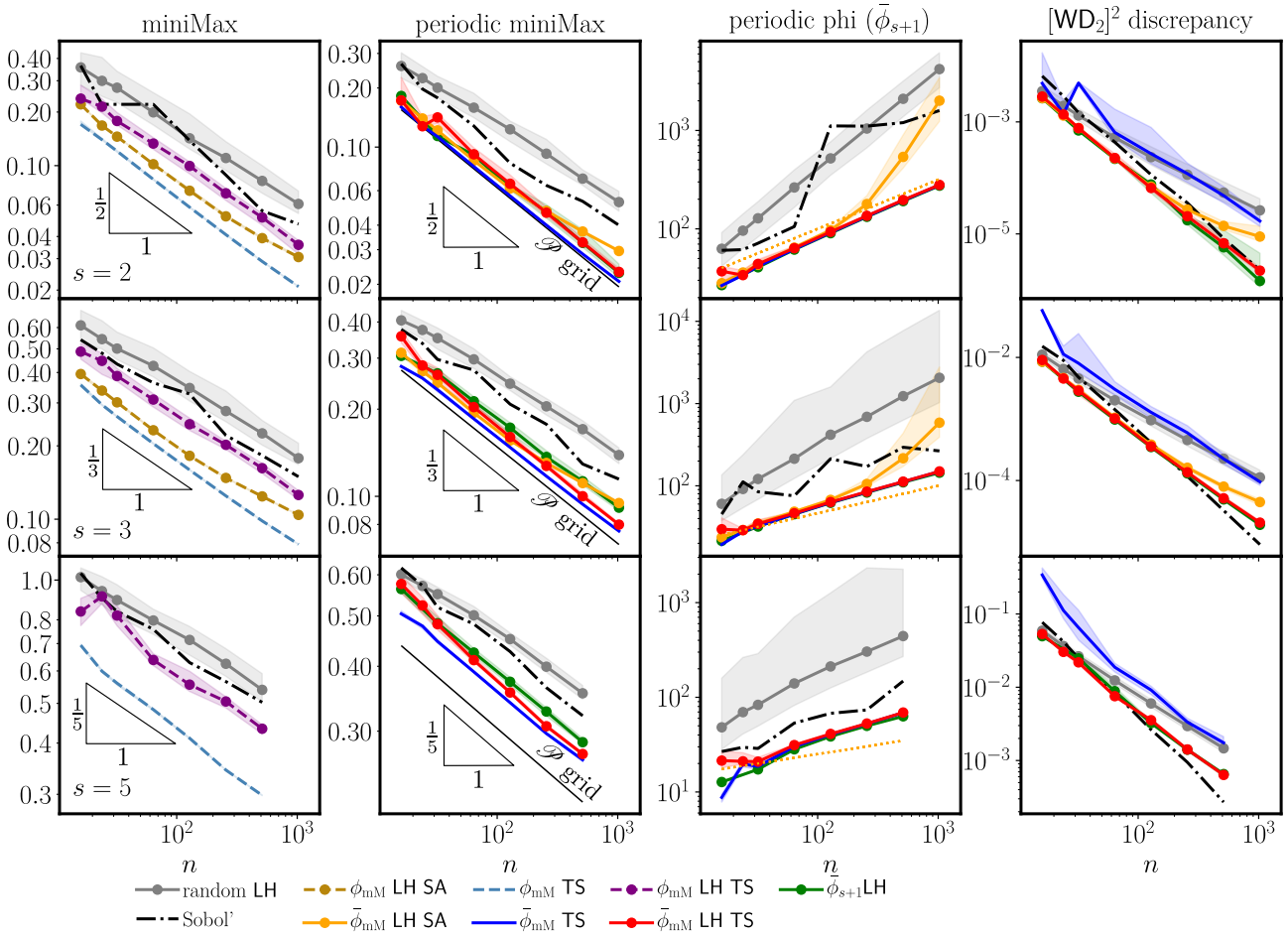

Figure 7: Medians (thick solid lines) and 5th-95th percentiles (shaded areas) of intersite minimax, periodic minimax, phi and wrap around L_2 discrepancy criteria computed on designs optimized with respect to different criteria and via different optimization methods. Three cases are considered: $s = 2$ (top row), 3 (central row) and 5 (bottom row). All LH designs are marked with solid circles.

Fig. 7 shows medians and 5th and 95th percentiles of the minimax (left), periodic minimax, periodic phi and wrap around L_2 discrepancy (right column) criteria values calculated based on $r = 100$ optimized designs in 2 and 3 dimensions. In 5 dimensions, the number of designs is $r = 50$.

The proposed time-stepping algorithm delivers the best results in both the minimax and periodic minimax cases. After latinization, these designs become worse as the latinization does not seek the optimal LH design. This is emphasized for the intersite minimax value. The simulated annealing optimization performs better than latinized time-stepping for low n as it is able to find the optimum among all LH designs. As n grows, simulated annealing with a reduced cooling schedule becomes too inefficient to deliver designs that perform well. Aside from the random LH designs, the QMC sequence is the worst design under comparison, though on the other hand it is capable of generating designs fast and simply, and provides the option to repetitively extend the sample size n.

The periodic phi optimal LH designs show a relatively low periodic minimax value considering they were not optimized with respect to this criterion. More interestingly, the periodic phi value of the compared designs is almost identical for (i) both raw and latinized minimax designs optimized by the time-stepping algorithm and (ii) periodic phi optimal LH designs. This confirms our hypothesis about the good *sample uniformity* of the periodic minimax designs.

The wrap around L_2 discrepancy (WD_2), evaluated in the last column of Fig. 7, measures the difference between the empirical distribution function associated with the design $\mathcal{D}$ and the uniform distribution over $\mathcal{U}$ [15]. As shown in [49], the WD_2 criterion favors *statistically uniform* designs. Fig. 7 shows that the discrepancies of the $\bar{\phi}_{\mathrm{mM}}$-optimized LH designs (periodic minimax LHDs) are very low; these designs are outperformed by the QMC for higher n in higher dimensions only, i.e., by sequences that have been purposely developed to have low discrepancy.

Finally, we derive the conservative lower limit of the minimax criterion as the radius of the hypersphere circumscribed to a simplex of a regular grid, denoted as $\mathcal{P}$. The grid itself is thoroughly described in the

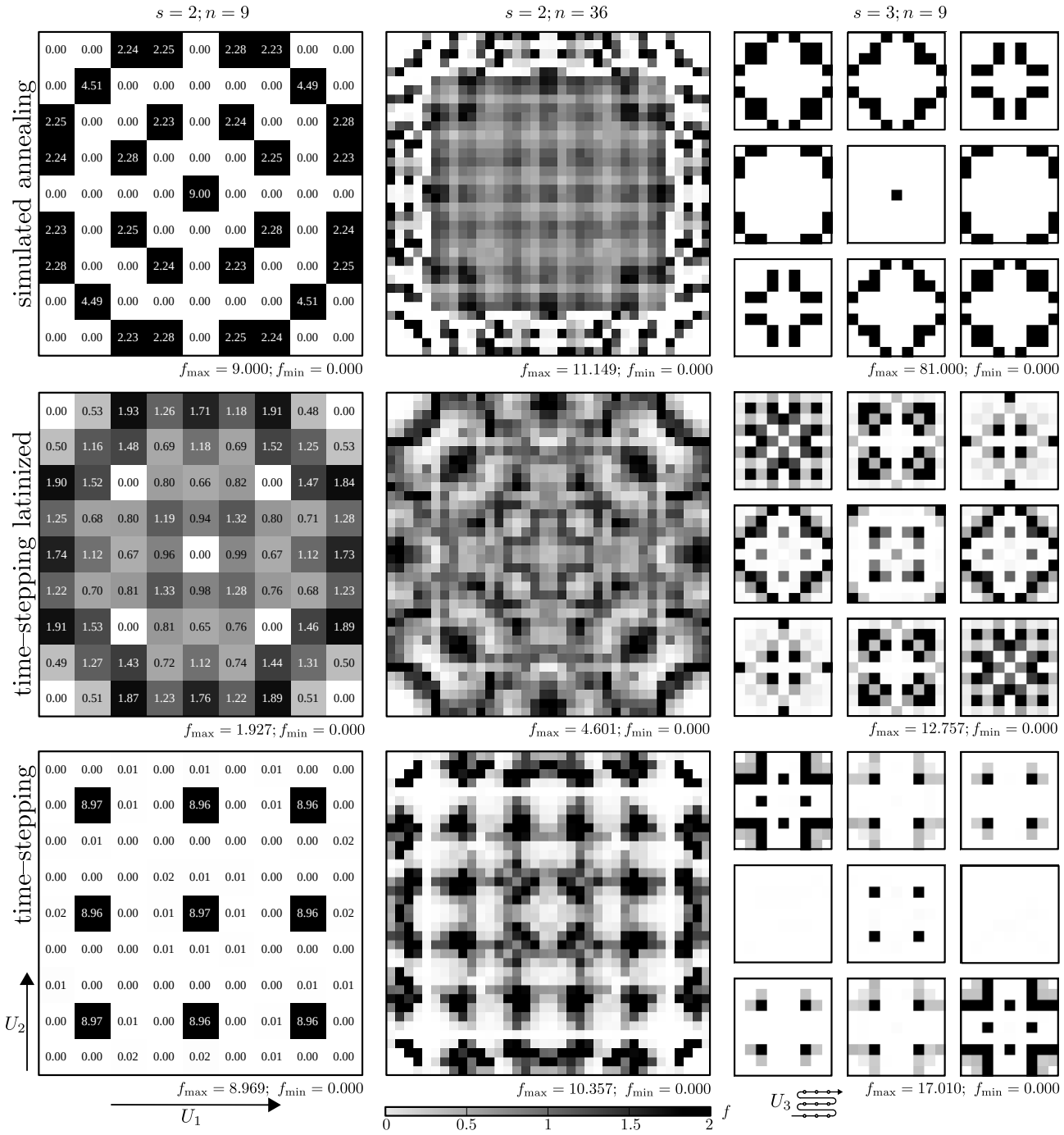

Figure 8: Relative frequencies f of sampling calculated by the optimization of $r = 10^4$ LH designs with respect to the intersite minimax (ϕ_{mM}) criterion. The top row shows histograms obtained by simulated annealing optimization, the bottom row histograms generated via a raw time-stepping procedure without latinization, and the central row histograms obtained by latinizing the time-stepping solution.

Appendix of [51]. The radius reads

$$\phi_{\mathrm{mM}}(\mathcal{P}) = \frac{\sqrt{s}\,\ell_{\mathrm{char}}}{\sqrt[s]{(s+1)^{s+1}}} = \frac{\sqrt{s}}{\sqrt[s]{(s+1)^{s+1}}}\,\frac{1}{\sqrt[s]{n}} \tag{9}$$

Fig. 7 shows that the $\bar{\phi}_{\mathrm{mM}}$ TS designs are very close to that theoretical limit in two dimensions. In three and five dimensions, the inevitable stretching of the ideal $\mathcal{P}$ grid leads to greater deviations from the theoretical limit. In any case, the best possible rate of decrease is maintained: $\bar{\phi}_{\mathrm{mM}}\mathsf{TS} \propto n^{-1/s}$; see the triangles in Fig. 7 that mark the exponents of power laws by the slopes of the straight lines.

6. Statistical uniformity of ϕ_{mM} and $\overline{\phi}_{\mathrm{mM}}$ optimal designs

In order to assess the statistical (non)uniformity, we generated ϕ_{mM} optimal designs via the simulated annealing process and also via the time-stepping algorithm $r = 10\,000$ times. The domain was divided into bins

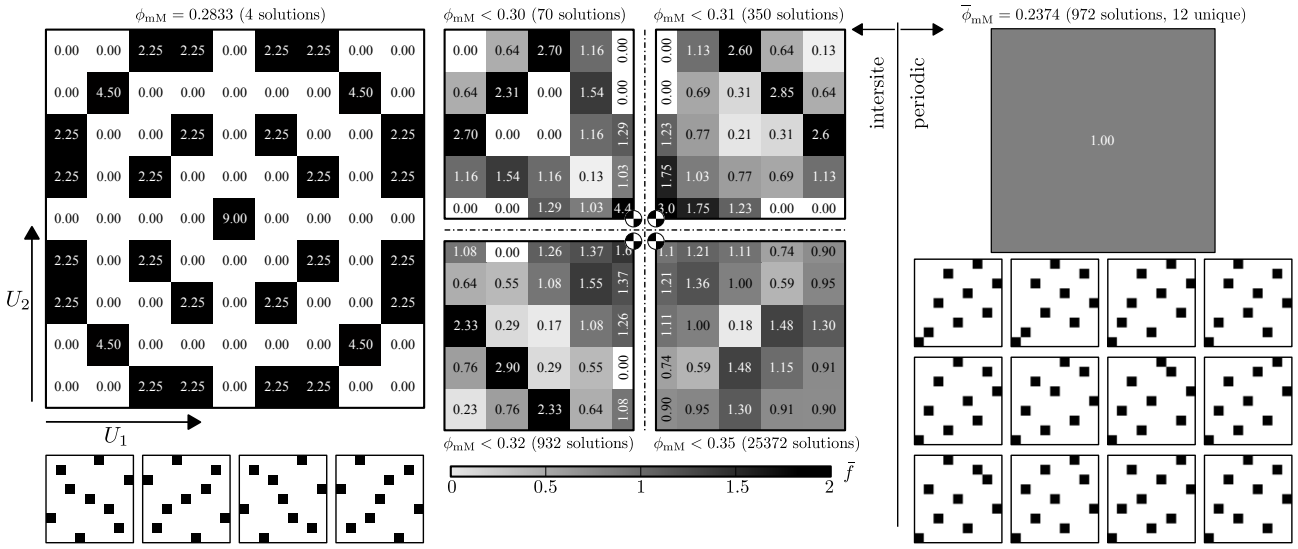

Figure 9: Relative frequencies f calculated for LH-sample sets with the minimax (ϕ_{mM}) and periodic minimax ($\overline{\phi}_{\mathrm{mM}}$) criteria for $n = 9$ and $s = 2$ based on optimal solutions found by an exhaustive search; left: map created by four optimal solutions for ϕ_{mM}(compare with the "less accurate" solution in Fig. 8, top left); middle: maps constructed from solutions with $\phi_{\mathrm{Mm}} \leq 0.30$, 0.31, 0.32 or 0.35; right: an ideally uniform map for the periodic version ($\overline{\phi}_{\mathrm{Mm}}$) along with all 12 unique solutions.

(the LH bins were used directly) and we calculated the absolute frequency, f, of sampling each bin over these r designs. If the criterion is *statistically uniform*, all the bins shall, for large r, share the same absolute frequency, which should be equal to the total number of sampled design points rn divided by the number of bins n^s. We therefore calculated and plotted the relative sampling frequency, which is the absolute frequency divided by the ideal one

$$f = \overline{f}\left(\frac{rn}{n^s}\right)^{-1} = \overline{f}\frac{n^{s-1}}{r} \tag{10}$$

For a statistically uniform design, $\lim_{r\to\infty} f = 1$ for all bins. The results of the analysis for $s = 2$ and $n \in \{9, 36\}$ and also $s = 3$ and $n = 9$ are plotted in Fig. 8 for designs optimized by simulated annealing (top row), time-stepping algorithm (bottom row) and time-stepping algorithm with latinization (central row). The figure confirms that the usage of the intersite metric produces strongly statistically nonuniform designs. When histograms from LH designs optimized with respect to the ϕ_{mM} criterion are compared with those of Audze-Eglājs, ϕ_p or ϕ_{Mm} from [9, 49], similar patterns appear. The corners are strongly undersampled, and then there are usually (hyper) sphere-like patterns of alternating oversampled and undersampled regions. Empty corners are also visible in Fig. 1 (top row), where periodic repetitions of a design are plotted.

Fig. 8 also shows that designs delivered by simulated annealing and the time-stepping algorithm are quite different. Time-stepping optimization is performed in $\mathcal{U}$ space, and subsequently the optimal solution is projected into $\mathcal{L}$ space by latinization. The latinization unfortunately deforms the optimal designs to create suboptimal LH designs with a high degree of randomness. Therefore, the histograms of latinized time-stepping solutions exhibit less contrast compared to histograms obtained with the help of simulated annealing.

The same maps can also be plotted for $\overline{\phi}_{\mathrm{mM}}$ designs. However, for this statistically uniform criterion, the maps are just uniformly gray with small random fluctuations of relative frequency around 1. The fluctuations decrease with r. In other words, the periodic criterion delivers *statistically uniform* designs.

For small enough problems (low n and s) it is possible to run an exhaustive search through the complete set of all possible LH designs and select those with minimum ϕ_{mM} or $\overline{\phi}_{\mathrm{mM}}$. van Dam [47] completed an exhaustive search for the minimax design with Euclidean intersite metric in two dimensions up to $n = 27$; the results are available at https://spacefillingdesigns.nl.

We present the results from our exhaustive search for both ϕ_{mM} and $\overline{\phi}_{\mathrm{mM}}$ criteria in Fig. 9 for $s = 2$ and $n = 9$. In case of the periodic metric, there are 972 LH designs for which $\overline{\phi}_{\mathrm{mM}}(\mathcal{D}) = 0.2374$. When the histogram is plotted, a perfectly uniform frequency map on the right hand side of Fig. 9 is obtained. All the LH bins are sampled with the same probability thanks to the shift invariance of the proposed $\overline{\phi}_{\mathrm{mM}}$ criterion. Indeed, among these 972 designs, only 12 are unique – none of them can be obtained by shifting the others. They are plotted in the bottom part of the right hand side of Fig. 9. Each of the 12 designs can be shifted 81 times (9 times along each direction) within the LH-class restriction. In this specific case, each of the shifted designs is different, and therefore $81 \times 12 = 972$ solutions are found in total.

For the intersite metric the ϕ_{mM} criterion provides four optimal solutions that are plotted at the bottom on the left hand side of Fig. 9. One can see that they are essentially only one solution flipped along the horizontal and/or vertical axis. The histogram constructed from them (the map above them) is almost identical to the

frequency map obtained by simulated annealing (Fig. 8 top left), proving that the optimization algorithm is capable of finding the global minimum in this case. However, such excellent optimization behavior can hardly be expected for greater n or s. Assuming that the optimization algorithm was terminated before the global optimum was found, the set of obtained nearly optimal solutions would be richer. This can be mimicked by also accepting nearly optimal solutions during the exhaustive search. The central part of Fig. 9 shows symmetric quarters of the frequency maps plotted for the acceptance bounds $\phi_{\mathrm{mM}} < 0.30$, 0.31, 0.32 and 0.35. The number of solutions quickly grows and the histogram becomes more uniform. Therefore, if poor cooling schedule settings are used in simulated annealing optimization, a more *statistically uniform* design set is expected (leading to a lower integration bias); however, worse *sample uniformity* should be expected and therefore also higher estimation variance.

7. Application to the integration of analytical functions

In this and the next section, the designs optimized according to various criteria are used to integrate functions in probability space. These functions are simple analytical functions which are easy to evaluate. Moreover they can be integrated analytically so we can determine error of the numerical integration and compare this error to find out which criterion provides the best designs. However, the realistic example of application would be some complex finite element solution of mechanical or diffusion problem with random inputs. But such a function would not allow us to determine the integration error as the exact integral cannot be computed. Nevertheless, the experience shows [48] that majority of engineering problems are smooth functions and conclusions obtained with simple analytical transformations hold also for most of the complicated simulation models formed, e.g., by the finite element method.

We selected three analytical functions to be numerically integrated over the unit hypercube. All of them are functions of an input vector $\boldsymbol{U}$ consisting of s independent variables uniformly distributed over the interval from 0 to 1.

$$g_{\mathrm{exp}}\left(\boldsymbol{U}\right) = \sum_{v=1}^{s} \exp\left[-\left(\Phi^{-1}(U_v)\right)^2\right] \tag{11}$$

$$g_{\mathrm{prod}}(\boldsymbol{U}) = \prod_{v=1}^{s} \Phi^{-1}(U_v) \tag{12}$$

$$g_{\mathrm{sob}}(\boldsymbol{U}) = \prod_{v=1}^{s} \frac{|4U_v - 2| + c_v}{1 + c_v} \tag{13}$$

The first two functions are taken from [9, 48]; they actually use independent standard Gaussian variables X_v as they employ memoryless transformation through the inverse Gaussian distribution function: $X_v = \Phi^{-1}(U_v)$. The last function, often used in sensitivity analysis [4], is called the Sobol' function. We choose c_v to be Fibonacci numbers.

One can easily compute the exact mean and standard deviation of these three functions

$$\mu_{\mathrm{exp}} \approx 0.577\, s \qquad \sigma_{\mathrm{exp}} \approx 0.337\, \sqrt{s} \tag{14a}$$

$$\mu_{\mathrm{prod}} = 0 \qquad \sigma_{\mathrm{prod}} = 1 \tag{14b}$$

$$\mu_{\mathrm{sob}} = 1 \qquad \sigma_{\mathrm{sob}} = \sqrt{-1 + \prod_{v=1}^{s}\left[\frac{1}{3(c_v+1)^2} + 1\right]} \tag{14c}$$

The numerical estimation of these variables is performed according to Eq. (2). The mean values and standard deviations are estimated via the standard point estimators

$$\hat{\mu}_{\mathrm{G}}(\mathcal{D}) \approx \frac{1}{n}\sum_{i=1}^{n} g_{\mathrm{G}}(\boldsymbol{u}_i) \tag{15}$$

$$\hat{\sigma}_{\mathrm{G}}(\mathcal{D}) \approx \sqrt{\frac{1}{n-1}\sum_{i=1}^{n}\left[g_{\mathrm{G}}(\boldsymbol{u}_i) - \hat{\mu}_{\mathrm{G}}(\mathcal{D})\right]^2} \tag{16}$$

We are interested in the error of such an estimation $\epsilon_I = |I - \hat{I}|$ where I and $\hat{I}$ represent the exact and estimated value of a particular quantity, respectively. The errors computed with the help of optimized designs are shown in Fig. 10 for the standard deviation of the exponential and product functions, and the mean value of the Sobol' function. The designs under comparison are the same as in Section 5.3, except the periodic phi designs ($\overline{\phi}_{s+1}$) are omitted. The median and 5th-95th percentiles of the error based on $r = 50 - 100$ designs are plotted.

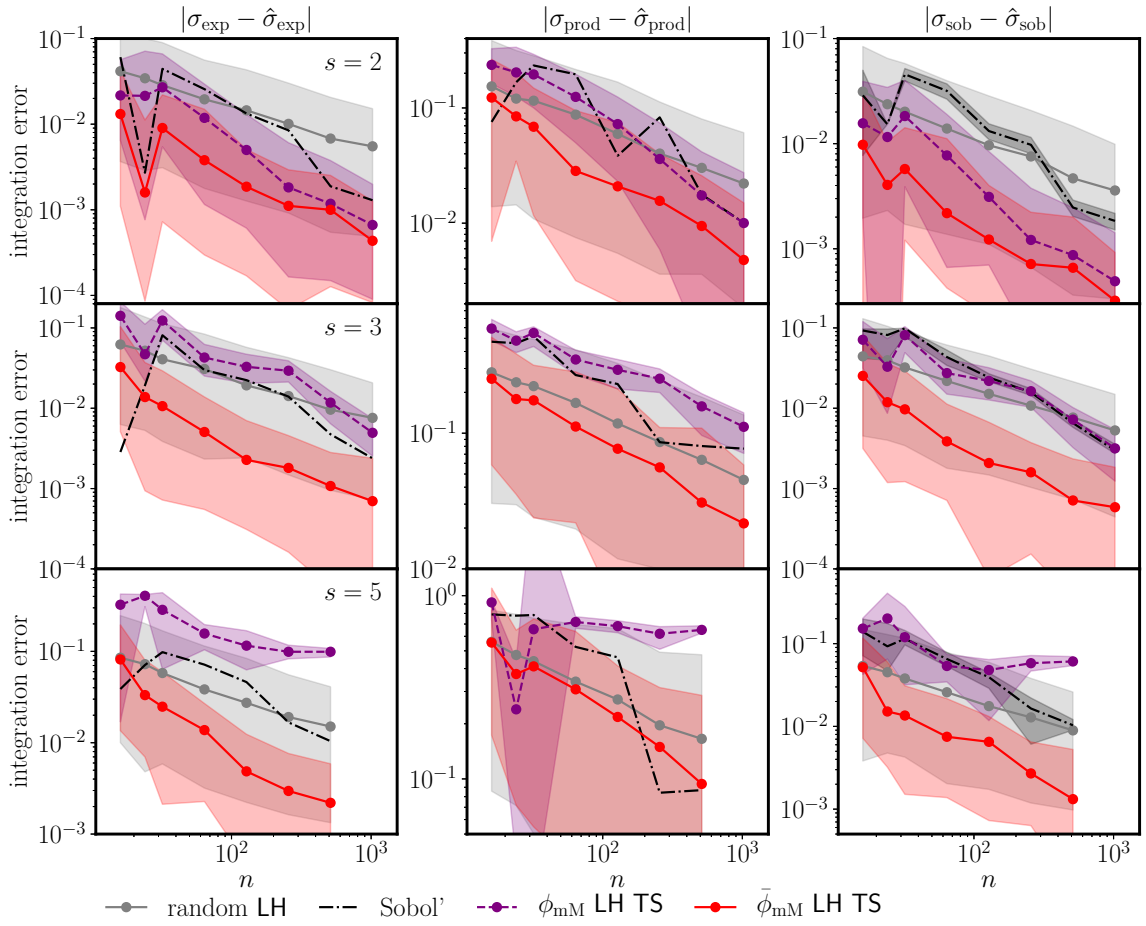

Figure 10: Convergence of integration errors for three simple analytical functions in 2, 3 and 5 dimensions for various design criteria. The lines represent medians and the shaded areas ranges from the 5th to 95th percentile. All LH designs are marked by solid circles.

- The reference random LH designs exhibit large integration error accompanied by large error variance, because the space-filling property is not optimized.
- The QMC sequence sometimes shows excellent behavior with the lowest error, but also often exhibits very large errors. Which of these scenarios occur seems to be unpredictable. Since there is just a single design for each n, there is no variance associated with QMC when studied on Eqs. (11) and (12). Eq. (13) is, however, sensitive to permutation of variables. We therefore computed the numerical integral for all possible permutations of variables and reported the median and percentiles from these results.
- The ϕ_{mM} criterion delivers designs with relatively low error variance but a large error median. The lack of statistical uniformity gives rise to bias in the integration that is revealed here. In some cases (for example for σ_{prod} error in 3 dimensions) the designs perform surprisingly well, but we attribute this to randomly occurring incidents in which there is a good correspondence between the integrated function and a coincidentally suitable pattern in the design. However, in most cases their error is greater than the average error of random LH designs. Fig. 10 shows results for only one construction method (ϕ_{mM} LH TS), the other methods (ϕ_{mM} TS and ϕ_{mM} LH SA) provide qualitatively similar results. Because these designs are strongly biased, we have eliminated them from further consideration.
- The best designs seem to be the proposed $\bar{\phi}_{\text{mM}}$ designs. They deliver low errors and also stable convergence (robustness). Only results for the latinized time-stepping contruction method are shown ($\bar{\phi}_{\text{mM}}$ LH TS designs). The raw designs from time-stepping optimization ($\bar{\phi}_{\text{mM}}$ TS) give similar results for exponential and product functions, but the latinized designs are better in the case of the Sobol' function, which apparently takes advantage of the LH restriction. The designs optimized via simulated annealing ($\bar{\phi}_{\text{mM}}$ LH SA) are also omitted. They are good for low n but become worse for large n due to the insufficient cooling schedule.

8. Integration of the subspace formed by Chebyshev polynomials

The robustness of numerical integration can only be fully revealed by testing a large number of different functions. We selected functions formed by Chebyshev polynomials of the first kind. These polynomials can be

defined by simple recursion on interval $u \in \langle -1, 1 \rangle$. Combined with mapping to our interval of interest $\langle 0, 1 \rangle$, the recursion yields

$$T_0(u) = 1 \tag{17}$$
$$T_1(u) = 2u - 1 \tag{18}$$
$$T_k(u) = 2(2u-1)T_{k-1}(u) - T_{k-2}(u) \tag{19}$$

These polynomials form an orthogonal basis on $\langle 0, 1 \rangle$; arbitrary function $f(u)$ can be written as an infinite sum or approximated by a finite sum

$$g(u) = \sum_{k=0}^{\infty} a_k T_k(u) \approx \sum_{k=0}^{K} a_k T_k(u) \tag{20}$$

where K is the truncation threshold and a_k are coefficients associated with the particular basis polynomial.

The extension of this concept into an s dimensional unit hypercube is straightforward. Our basis functions are now s dimensional products of unidimensional polynomials of arbitrary order

$$g(\boldsymbol{u}) = \sum_{\boldsymbol{k}} a_{\boldsymbol{k}} T_{\boldsymbol{k}}(\boldsymbol{u}) \approx \sum_{\boldsymbol{k}}^{K} a_{\boldsymbol{k}} T_{\boldsymbol{k}}(\boldsymbol{u}) \tag{21}$$

$$\text{where} \quad T_{\boldsymbol{k}}(\boldsymbol{u}) = \prod_{v=1}^{s} T_{k_v}(u_v) \tag{22}$$

$\boldsymbol{k}$ is a vector of integers collecting orders of individual unidimensional polynomials. Considering only integers up to threshold K (as symbolically denoted in the second summation of Eq. (21)), the infinite series is truncated and $g(\boldsymbol{u})$ is only approximated.

The integration of individual unidimensional Chebyshev polynomials can be performed analytically

$$\int_0^1 T_k(u)\,\mathrm{d}u = \begin{cases} 0 & \text{for odd } k \\ \frac{1}{1-k^2} & \text{for even } k \end{cases} \tag{23}$$

and the integration of multidimensional polynomials is the product of unidimensional integrals

$$I_{\boldsymbol{k}} = \int_{[0,1]^s} T_{\boldsymbol{k}}(\boldsymbol{u})\,\mathrm{d}\boldsymbol{u} = \prod_{v=1}^{s} \int_0^1 T_{k_v}(u_v)\,\mathrm{d}u_v \tag{24}$$

The integration of any function represented by the multidimensional Chebyshev basis then transforms into the summation of basis integrals weighted by the coefficients

$$I_g = \int_{[0,1]^s} g(\boldsymbol{u})\,\mathrm{d}u \approx \sum_{\boldsymbol{k}}^{K} a_{\boldsymbol{k}} I_{\boldsymbol{k}} \tag{25}$$

Estimation of the same integral using a given design $\mathcal{D}$ with n points reads

$$\hat{I}_g(\mathcal{D}) \approx \sum_{\boldsymbol{k}}^{K} a_{\boldsymbol{k}} \hat{I}_{\boldsymbol{k}}(\mathcal{D}) \tag{26}$$

$$\text{where} \quad \hat{I}_{\boldsymbol{k}}(\mathcal{D}) = \frac{1}{n} \sum_{i=1}^{n} T_{\boldsymbol{k}}(\boldsymbol{u}_i) \tag{27}$$

The error of the numerical integration is bounded by a linear combination of errors due to numerical integration of individual basis terms.

$$\epsilon_I(\mathcal{D}) = |I_g - \hat{I}_g| \leq \sum_{\boldsymbol{k}}^{K} |a_{\boldsymbol{k}}| \epsilon_{\boldsymbol{k}}(\mathcal{D}) \tag{28}$$

$$\text{where} \quad \epsilon_{\boldsymbol{k}}(\mathcal{D}) = |I_{\boldsymbol{k}} - \hat{I}_{\boldsymbol{k}}| \tag{29}$$

Any design that integrates basis polynomials well also performs well when integrating an arbitrary function obtained from the linear combination of the basis. The robustness of the periodic minimax design during integration is therefore demonstrated by its ability to integrate basis polynomials well.

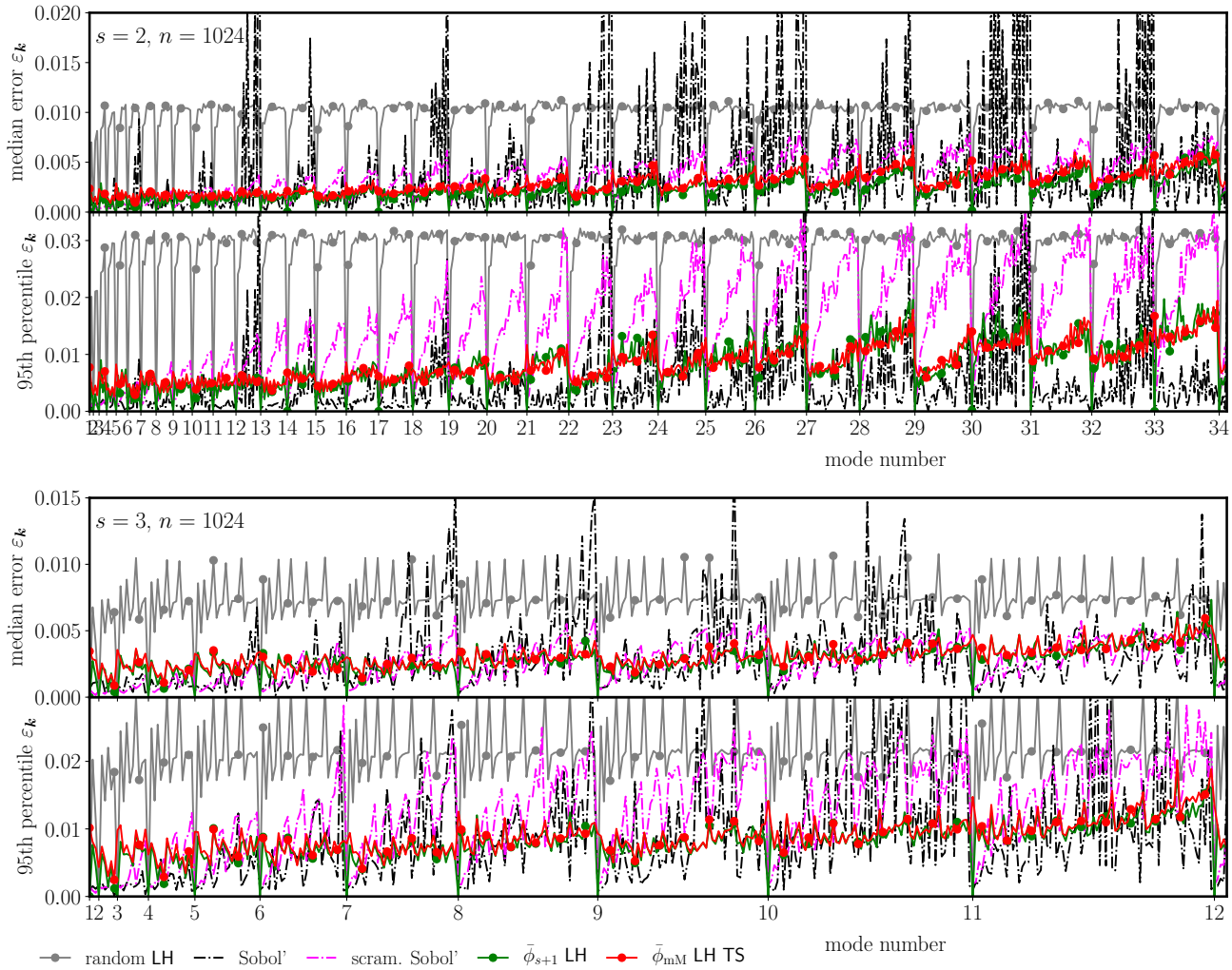

Figure 11: Integration error evaluated using Chebyshev polynomials for $s = 2, 3$ integrated by a design of 1024 points optimized with respect to various criteria.

We consider $K = \lceil \sqrt[s]{n} \rceil$ to be the maximum polynomial order for which integration error is measured. For higher K, polynomials have more changes of signs inside the interval $\langle 0, 1 \rangle$ than the total number of points used for integration. Therefore, one can hardly expect good performance for $K > \lceil \sqrt[s]{n} \rceil$.

The performance of a design should not depend on the order of modes; we would like to see the same performance for arbitrary permutations of $\boldsymbol{k}$. For that reason, we always integrate all permutations of $\boldsymbol{k}$ and report the statistical data. Only sorted vectors $\boldsymbol{k}$ are therefore used, i.e., $\boldsymbol{k} = \{1, 1, 2\}$ actually represents all 3 different permutations $\{1, 1, 2\}$, $\{2, 1, 1\}$ and $\{1, 2, 1\}$. We can also order all the sorted $\boldsymbol{k}$ that have no item greater than $\lceil \sqrt[s]{n} \rceil$ in the following way: $\boldsymbol{k}_a \leq \boldsymbol{k}_b \Leftrightarrow \forall v : k_v^a \leq k_v^b$.

Fig. 11 shows integration performance in dimensions two and three for different mode vectors $\boldsymbol{k}$ using $n = 1024$ points. Separate graphs are shown for the median of the error (top graph) and the 95th percentile (bottom graph). We eliminated all the non-periodic designs from the comparison since we had already shown that they result in strong bias. We also omitted the $\overline{\phi}_{\mathrm{mM}}$ design generated by simulated annealing ($\bar{\phi}_{\mathrm{mM}}$ LH SA), since for this large number of points shuffling optimization already suffers from an insufficient number of trial swaps. For the sake of clarity, we did not plot *latinized* $\overline{\phi}_{\mathrm{mM}}$ designs generated via the time-stepping process ($\bar{\phi}_{\mathrm{mM}}$ LH TS) because they exhibit behavior almost distinguishable from *raw* time-stepping ($\bar{\phi}_{\mathrm{mM}}$ TS) designs. The only difference is at modes where all the $\boldsymbol{k}$ items are zero except the last one, for example (0, 3), (0, 8) or (0, 0, 7). For these *single-degree* mode vectors, the Chebyshev basis $T_{\boldsymbol{k}}$ is dependent on a single variable only, and therefore the LH property becomes extremely advantageous. These modes are located in Fig. 11 at the ticks of the horizontal axis labeled by the single nonzero integer in the vector $\boldsymbol{k}$. At these particular locations, the latinized time-stepping generated $\overline{\phi}_{\mathrm{mM}}$ designs exhibit significantly lower integration error compared to the raw ones plotted.

Let us now comment on the individual curves shown in Fig. 11:

- The reference solution is again provided by the random LH designs. They exhibit large error and also large variance. However, the error suddenly drops for the single-degree mode vector thanks to the LH restriction.

- The QMC Sobol' sequences integrate with low errors for initial mode vectors, but the integration errors quickly increase and they often even exceed the random LH design error.
- Numerical integration is often performed with re-randomized QMC sequences in the literature. For comparison purposed, we included scrambled Sobol' sequence using two types of scrambling: Owen scrambling [33] and also the Faure-Tezuka [45] type of scrambling; see also [18]. The median performance is more stable, however, 95th percentile of error is relatively large which is a price paid for the re-randomization.
- The periodic phi criterion (described in [49]) shows excellent performance. These LH designs have the lowest error from all of those presented, and also their variance seems to be the lowest.
- Finally, the $\overline{\phi}_{\mathrm{mM}}$ designs developed here via time-stepping are just a little bit worse than the phi designs. If the latinized version of these designs were used, we would also obtain diminishing integration errors for the single-degree mode vectors.

Along with the phi criterion, the $\overline{\phi}_{\mathrm{mM}}$ criterion (with a proper optimization method) is capable of delivering robust designs that integrate all the basis functions with low error and low error variability. They are outperformed only for low Chebyshev modes by QMC sequences because these sequences are purposely prepared in order to integrate very smooth functions well [8].

9. Conclusions

The designs optimized with respect to the standard (intersite) minimax distance are *statistically nonuniform* and thus yield systematically biased estimators when used for numerical Monte Carlo type integration. When the intersite distance is replaced by the periodic metric, the *statistical uniformity* is guaranteed and unbiased estimators are obtained. The reduction of estimator variance is achieved by excellent space-filling property and discrepancy (and thus also *sample uniformity*) of the minimax and periodic minimax optimal designs.

The numerical integration is tested using three simple analytical functions and thousands of functions generated in the space of multidimensional Chebyshev polynomials. In all the tests, the periodic minimax designs exhibited low integration error. They are sometimes outperformed by quasi Monte Carlo sequences (represented by the Sobol' sequence), but these sequences often exhibit extremely large errors (greater than those obtained from random LH designs). The excellent and stable integration ability (robustness) of the minimax designs makes them the best choice (along with the phi designs included for comparison).

A disadvantage of the (periodic) minimax criterion is its extremely large computational complexity. In an attempt to speed up the calculations, we have developed a method employing the incremental construction of (periodic) Voronoï tessellation. The computational time is however still excessive and prohibits the use of the otherwise reliable shuffling optimization method based on simulated annealing. Instead, a novel time-stepping algorithm has been developed to deliver $\overline{\phi}_{\mathrm{mM}}$ optimized designs in reasonable time. Even with these algorithms, one can hardly imagine the use of this design criterion in dimensions greater than five.

Acknowledgement

The authors acknowledge the financial support provided by the Czech Science Foundation under projects Nos. GA19-12197S and GC19-06684J.

References

[1] P. Audze and Vilnis Eglājs. New approach for planning out of experiments. *Problems of Dynamics and Strengths*, 35:104–107, 1977. (in Russian).

[2] C. Bradford Barber, David P. Dobkin, and Hannu Huhdanpaa. The quickhull algorithm for convex hulls. *ACM Trans. Math. Softw.*, 22(4):469–483, 1996. ISSN 0098-3500. doi: 10.1145/235815.235821.

[3] Mohamed Amine Bouhlel, John T. Hwang, Nathalie Bartoli, Rémi Lafage, Joseph Morlier, and Joaquim R.R.A. Martins. A Python surrogate modeling framework with derivatives. *Advances in Engineering Software*, 135:102662, 2019. ISSN 0965-9978. doi: 10.1016/j.advengsoft.2019.03.005.

[4] Evgeny Burnaev, Ivan Panin, and Bruno Sudret. Efficient design of experiments for sensitivity analysis based on polynomial chaos expansions. *Annals of Mathematics and Artificial Intelligence*, 81(1):187–207, 2017. ISSN 1573-7470. doi: 10.1007/s10472-017-9542-1.

[5] V. Černý. Thermodynamical approach to the traveling salesman problem: An efficient simulation algorithm. *Journal of Optimization Theory and Applications*, 45(1):41–51, 1985. ISSN 1573-2878. doi: 10.1007/BF00940812.

[6] W.J. Conover. On a better method for selecting input variables. unpublished Los Alamos National Laboratories manuscript, reproduced as Appendix A of "Latin Hypercube Sampling and the Propagation of Uncertainty in Analyses of Complex Systems" by J.C. Helton and F.J. Davis, Sandia National Laboratories report SAND2001-0417, 1975.

[7] Jorge Cortés and Francesco Bullo. Nonsmooth coordination and geometric optimization via distributed dynamical systems. *SIAM Review*, 51(1):163–189, 2009. ISSN 00361445, 10957200.

[8] Josef Dick. Higher order scrambled digital nets achieve the optimal rate of the root mean square error for smooth integrands. *The Annals of Statistics*, 39(3):1372–1398, 2011. ISSN 00905364. doi: 10.1214/11-AOS880.

[9] Jan Eliáš and M. Vořechovský. Modification of the Audze–Eglājs criterion to achieve a uniform distribution of sampling points. *Advances in Engineering Software*, 100:82–96, 2016. doi: 10.1016/j.advengsoft.2016.07.004.
[10] Kai-Tai Fang and Y. Wang. *Number-Theoretic Methods in Statistics*. Chapman and Hall/CRC, London ; New York, 1st edition edition, 1993. ISBN 9780412465208.
[11] Fabian Fuerle and Johann Sienz. Formulation of the Audze-Eglais uniform latin hypercube design of experiments for constrained design spaces. *Advances in Engineering Software*, 42(9):680–689, 2011. ISSN 0965-9978. doi: 10.1016/j.advengsoft.2011.05.004.
[12] Sushant S. Garud, Iftekhar A. Karimi, and Markus Kraft. Design of computer experiments: A review. *Computers & Chemical Engineering*, 106:71–95, 2017. ISSN 0098-1354. doi: 10.1016/j.compchemeng.2017.05.010.
[13] Arnaud Guyader, Nicolas Hengartner, and Eric Matzner-Løber. Simulation and estimation of extreme quantiles and extreme probabilities. *Applied Mathematics & Optimization*, 64(2):171–196, 2011. ISSN 1432-0606. doi: 10.1007/s00245-011-9135-z.
[14] J.H. Halton. On the efficiency of certain quasi-random sequences of points in evaluating multi-dimensional integrals. *Numerische Mathematik*, 2(1):84–90, 1960. ISSN 0029-599X. doi: 10.1007/BF01386213.
[15] Fred J. Hickernell. Lattice rules: How well do they measure up? In Peter Hellekalek and Gerhard Larcher, editors, *Random and Quasi-Random Point Sets*, chapter Lattice Rules: How Well Do They Measure Up?, pages 109–166. Springer New York, New York, NY, 1998. ISBN 978-1-4612-1702-2. doi: 10.1007/978-1-4612-1702-2_3.
[16] Fred J. Hickernell. A generalized discrepancy and quadrature error bound. *Mathematics of Computation*, 67(221):299–322, 1999. doi: 10.1090/S0025-5718-98-00894-1.
[17] Edmund Hlawka. Funktionen von beschränkter Variation in der Theorie der Gleichverteilung. *Annali di Matematica Pura ed Applicata*, 54(1):325–333, Dec 1961. ISSN 1618-1891. doi: 10.1007/BF02415361.
[18] Hee Sun Hong and Fred J. Hickernell. Algorithm 823: Implementing scrambled digital sequences. *ACM Transactions on Mathematical Software*, 29(2):95–109, June 2003. ISSN 0098-3500. doi: 10.1145/779359.779360.
[19] M.E. Johnson, L.M. Moore, and D. Ylvisaker. Minimax and maximin distance designs. *Journal of Statistical Planning and Inference*, 2(26):131–148, 1990. ISSN 0378-3758. doi: 10.1016/0378-3758(90)90122-B.
[20] S. Kirkpatrick, C. D. Gelatt, and M. P. Vecchi. Optimization by simulated annealing. *Science*, 220(4598):671–680, 1983. ISSN 0036-8075. doi: 10.1126/science.220.4598.671.
[21] Ronald Kleiss and Achilleas Lazopoulos. Error in Monte Carlo, quasi-error in Quasi-Monte Carlo. *Computer Physics Communications*, 175(2):93–115, 2006. ISSN 0010-4655. doi: 10.1016/j.cpc.2006.02.001.
[22] J. F. Koksma. Een algemeene stelling uit de theorie der gelijkmatige verdeeling modulo 1. *Mathematica B*, 11:7–11, 1942/1943.
[23] Wang-Sheng Liu, Sai Hung Cheung, and Wen-Jun Cao. An efficient surrogate-aided importance sampling framework for reliability analysis. *Advances in Engineering Software*, 135:102687, 2019. ISSN 0965-9978. doi: 10.1016/j.advengsoft.2019.102687.
[24] Simon Mak and V. Roshan Joseph. Support points. *The Annals of Statistics*, 46(6A):2562–2592, 12 2018. doi: 10.1214/17-AOS1629.
[25] Jan Mašek and Miroslav Vořechovský. Parallel implementation of hyper-dimensional dynamical particle system on CUDA. *Advances in Engineering Software*, 125:178–187, 2018. ISSN 0965-9978. doi: 10.1016/j.advengsoft.2018.03.009.
[26] Jan Mašek and Miroslav Vořechovský. Approximation of Voronoï cell attributes using parallel solution. *Advances in Engineering Software*, 132:7–17, 2019. ISSN 0965-9978. doi: 10.1016/j.advengsoft.2019.03.012.
[27] M. D. McKay, W. J. Conover, and R. J. Beckman. A comparison of three methods for selecting values of input variables in the analysis of output from a computer code. *Technometrics*, 21:239–245, 1979. doi: 10.1080/00401706.1979.10489755.
[28] Max D. Morris and Toby J. Mitchell. Exploratory designs for computational experiments. *Journal of Statistical Planning and Inference*, 43(3):381–402, 1995. ISSN 0378-3758. doi: 10.1016/0378-3758(94)00035-T.
[29] H. Niederreiter. *Random Number Generation and Quasi-Monte Carlo Methods*. CBMS-NSF Regional Conference Series in Applied Mathematics. Society for Industrial and Applied Mathematics, Philadelphia, Pennsylvania, 1992. ISBN 978-0-898712-957.
[30] Harald Niederreiter. Point sets and sequences with small discrepancy. *Monatshefte für Mathematik*, 104:273–337, 1987. ISSN 0022-314X. doi: 10.1007/BF01294651.
[31] Harald Niederreiter. A quasi-monte carlo method for the approximate computation. *Journal of Number Theory*, 30(1):51–70, 1988. ISSN 0022-314X. doi: 10.1016/0022-314X(88)90025-X.
[32] Harald Niederreiter. Low-discrepancy and low-dispersion sequences. *Journal of Number Theory*, 30(1):51–70, 1988. ISSN 0022-314X. doi: 10.1016/0022-314X(88)90025-X.
[33] Art B. Owen. Scrambling sobol' and niederreiter-xing points. *Journal of Complexity*, 14(4):466–489, 1998. ISSN 0885-064X. doi: 10.1006/jcom.1998.0487.
[34] Luc Pronzato. Minimax and maximin space-filling designs: some properties and methods for construction. *Journal de la Societe Française de Statistique*, 158(1):7–36, 2017.
[35] Luc Pronzato and Werner G. Müller. Design of computer experiments: space filling and beyond. *Statistics and Computing*, 22(3):681–701, 2012. ISSN 1573-1375. doi: 10.1007/s11222-011-9242-3.
[36] R Core Team. *R: A Language and Environment for Statistical Computing*. R Foundation for Statistical Computing, Vienna, Austria, 2013. URL `http://www.R-project.org/`.
[37] J. Andrew Royle and Doug Nychka. An algorithm for the construction of spatial coverage designs with implementation in SPLUS. *Comput. Geosci.*, 24(5):479–488, 1998. ISSN 0098-3004. doi: 10.1016/S0098-3004(98)00020-X.
[38] Chris H. Rycroft. VORO++: A three-dimensional Voronoi cell library in C++. *Chaos: An Interdisciplinary Journal of Nonlinear Science*, 19(4):041111, 2009. doi: 10.1063/1.3215722.
[39] Václav Sadílek and Miroslav Vořechovský. Evaluation of pairwise distances among points forming a regular orthogonal grid in a hypercube. *Journal of Civil Engineering and Management*, pages 410–423, 2019. ISSN 1392-3730. doi: 10.3846/jcem.2018.5189.
[40] Thomas J. Santner, Brian J. Williams, and William I. Notz. *The Design and Analysis of Computer Experiments*. Springer Series in Statistics. Springer-Verlag New York, 2003. ISBN 978-0-387-95420-2. doi: 10.1007/978-1-4757-3799-8.
[41] Michael D. Shields. Adaptive Monte Carlo analysis for strongly nonlinear stochastic systems. *Reliability Engineering & System Safety*, 175:207–224, 2018. ISSN 0951-8320. doi: 10.1016/j.ress.2018.03.018.
[42] Liang Shuai, Xiaohu Guo, and Miao Jin. GPU-based computation of discrete periodic centroidal Voronoi tessellation in hyperbolic space. *Computer-Aided Design*, 45(2):463–472, 2013. ISSN 0010-4485. doi: 10.1016/j.cad.2012.10.029.
[43] Matthias H. Y. Tan. Minimax designs for finite design regions. *Technometrics*, 55(3):346–358, 2013. doi: 10.1080/00401706.2013.804439.
[44] Stefano Tarantola, William Becker, and Dirk Zeitz. A comparison of two sampling methods for global sensitivity analysis. *Computer Physics Communications*, 183(5):1061–1072, 2012. ISSN 0010-4655. doi: 10.1016/j.cpc.2011.12.015.
[45] Shu Tezuka and Henri Faure. *i*-binomial scrambling of digital nets and sequences. *Journal of Complexity*, 19(6):744–757, December 2003. ISSN 0885-064X. doi: 10.1016/S0885-064X(03)00035-9.
[46] William Notz Thomas J. Santner, Brian J. Williams. *The Design and Analysis of Computer Experiments*. Springer Series in

Statistics. Springer-Verlag New York, 2003. ISBN 978-0-387-95420-2. doi: 10.1007/978-1-4757-3799-8.
[47] Edwin R. van Dam. Two-dimensional minimax Latin hypercube designs. *Discrete Applied Mathematics*, 156(18):3483–3493, 2008. ISSN 0166-218X. doi: 10.1016/j.dam.2008.02.009.
[48] M. Vořechovský. Hierarchical refinement of Latin Hypercube Samples. *Computer-Aided Civil and Infrastructure Engineering*, 30(5):394–411, 2015. ISSN 1467-8667. doi: 10.1111/mice.12088.
[49] M. Vořechovský and Jan Eliáš. Modification of the maximin and ϕ_p (phi) criteria to achieve statistically uniform distribution of sampling points. *Technometrics*, -(-):–, 2020. doi: 10.1080/00401706.2019.1639550. in press.
[50] M. Vořechovský and D. Novák. Correlation control in small sample Monte Carlo type simulations I: A Simulated Annealing approach. *Probabilistic Engineering Mechanics*, 24(3):452–462, 2009. ISSN 0266-8920. doi: 10.1016/j.probengmech.2009.01.004.
[51] Miroslav Vořechovský, Jan Mašek, and Jan Eliáš. Distance-based optimal sampling in a hypercube: Analogies to N-body systems. *Advances in Engineering Software*, 137:102709, 2019. ISSN 0951-8320. doi: 10.1016/j.advengsoft.2019.102709.
[52] Diethelm Wuertz, Tobias Setz, and Yohan Chalabi. *fOptions: Rmetrics – Pricing and Evaluating Basic Options*, 2017. R package, version 3.0.1.
[53] Dong-Ming Yan, Kai Wang, Bruno Lévy, and Laurent Alonso. Computing 2D Periodic Centroidal Voronoi Tessellation. In *8th International Symposium on Voronoi Diagrams in Science and Engineering - ISVD2011*, Qingdao, China, 2011. doi: 10.1109/ISVD.2011.31.
[54] Dong-Ming Yan, Wenping Wang, Bruno Lévy, and Yang Liu. Efficient computation of clipped Voronoi diagram for mesh generation. *Computer-Aided Design*, 45(4):843–852, 2013. ISSN 0010-4485. doi: 10.1016/j.cad.2011.09.004. Geometric Modeling and Processing 2010.